

Flexible model of water based on the dielectric and electromagnetic spectrum properties :

TIP4P/ ϵ_{Flex} .

Raúl Fuentes-Azcatl*

*Universidad Autónoma Metropolitana Unidad Xochimilco, Calzada del Hueso 1100,
CDMX, CP 04960, México*

E-mail: razcatl@correo.xoc.uam.mx

Abstract

The Infrared Spectrum is used as an experimental data target, to improved the TIP4P/ ϵ , adding harmonic potential $U(r)$ in all bonds and harmonic potential $U(\theta)$ in the angle formed by the hydrogens and oxygen atoms of the water molecule.

The flexibility in the molecule gives the ability of the water molecules to change, around different temperatures and pressures, their structure and in the bulk liquid the distribution of the dipole moment. This distribution helps to reproduce better the experimental data that the rigid models can not describe. The rigid water models of 3 and 4 sites have limitations to describe all the experimental properties, and is because can not take on how the dipole moment is distributed of dipole moment around the different thermodynamics phases.

The new flexible TIP4P/ ϵ_{Flex} water model is compared to the improve models of TIP4P and OPC model.

Introduction

The research of how the molecular interactions in water are related to its unique properties, is a fundamental and important subject in physical chemistry. A related essential question is how water interacts with solutes such as ions,^{1,2} organic molecules³ and proteins.⁴ These reasons are a field of study of water interactions and has been a highly active field for decades in experimental and theoretical chemistry.

Several interesting and successful interaction potentials (force fields, FF) have been developed in the last years.^{5,6} The simulation research had been showed that these FF take on for many important properties of liquid water, although, is there still space to improvement the rigid models?. Now a days the TIP4P/ ϵ ⁷ can reproduce better the experimental values than others.^{8,10}

In molecular simulations, solvents such as water are often represented by explicit models such as TIP3P or SPC/E.^{11,12} Many of these explicit-solvent models were originally developed

and parametrize a few decades ago. They were parametrize to agree with experimental data such as the density, self-diffusion coefficient and enthalpy of vaporization of liquid phase, key quantities that are readily available from accurate experiments. However, such molecular solvent models do not typically predict the correct experimental values of transport and dielectric properties.^{6,8,10} This is unfortunate because molecular simulations are so commonly used to treat the solvation of polar and charged molecules, for which it is essential that the solvent respond properly to electrostatic fields.

Since the TIP4P model¹¹ was improved, by adjusting the epsilon parameter of the Lenard-Jones potential to obtain an important improvement by the experimental properties able to reproduce, TIP4P/05 model.¹³ The search has continued to have a better model that reproduces more and better the experimental values at different pressure and temperature conditions.

By applying the dipole moment of minimum density method $\mu_{min,\rho}$ to the original TIP4P model, it was improved and was name TIP4P/ ϵ ^{7,8}(because reproduce the dielectric constant at different thermodynamics conditions), as well as the SPC model was improved with the same method and the SPC/ ϵ ⁹ was obtained. TIP4P/ ϵ model can reproduce the same experimental data as the TIP4P/05 and adds the reproduction of the experimentla values of the dielectric constant with a minimal of error¹⁰ and isothermal compressibility under various thermodynamic conditions. It seems that this model is the most optimal under this rigid 4-site scheme, as shown by the work of Wang et al,¹⁴ reaching very close parameters to the TIP4P/ ϵ with computational machine learning methods. Another effort to improve the TIP4P force field is the recent TIP4P-ST by Qiu et al;¹⁵ TIP4P-ST implement the method of Salas et al,¹⁶ using the surface tension as a target parameter. In this work these last two models are compared with the new TIP4P/ ϵ_{Flex}

A common feature of the most popular water models is that they are rigid non-polarizables, i.e., the intramolecular degrees of freedom are off.

It may seem obvious that a step forward for the improvement of the rigid non-polarizable

water potentials would be the addition of flexibility. However, there has been some skepticism in the past about the usefulness of flexible water models.¹⁷⁻²⁰ In fact, Tironi et al.¹⁸ concluded that the introduction of flexibility creates more problems than it solves and does not improve upon the accuracy of rigid models. It seems natural that the development of flexible models will consist of the addition of flexibility to a successful rigid potential.

A number of computer simulations with different flexible water models have been reported^{5,21-27} since the pioneering works of Lemberg and Stillinger²⁶ and Toukan and Rahman.²⁸

The dominant paradigm in water model development is to fit the parameters to reproduce a set of experimentally measured condensed phase properties. Generally speaking, a diverse data set over a wide range of thermodynamic conditions improve the domain of applicability of the model, but it also increases the complexity of the optimization problem.

The last proposal is the one made by Fuentes and Barbosa FAB/ ϵ ,³⁰ taking into account the flexibility through the addition of a harmonic potential in the OH bond and another in the HOH angle of a 3-body model, generating an improvement in the models of three sites. By adding the harmonic potential in the bond of a molecule such as CO₂, it has been possible to improve the reproduction of experimental values²⁹

The rest of the work is organized as follows: Section 2 gives the force field of TIP4P/ ϵ_{Flex} model of water, Section 3 search of parameters 4 gives the Results and in Section 5 the conclusions. Finally, references are given.

The force field of TIP4P/ ϵ_{Flex} model of water

As for the intermolecular potential, we used a four sites model like the usual choice of TIP4P model structures: a Lennard-Jones center at the position of the oxygen atom plus

the electrostatic interaction given by two positive charges located at the hydrogen atoms and a compensating negative charge placed at the so-called M-site. The water molecules have four sites: two hydrogens, an oxygen and a site M located at a distance l_{OM} from the oxygen atom along the bisector of the hydrogen atoms. The intramolecular interactions in the flexible model are defined by harmonic potentials in bonds and angle,

$$U(r) = \frac{k_r}{2}(r - r_0)^2 \quad \text{and} \quad U(\theta) = \frac{k_\theta}{2}(\theta - \theta_0)^2, \quad (1)$$

where r is the bond distance and θ is the bond angle. The subscript 0 denotes their equilibrium values, k_r and k_θ are the corresponding spring constants.

The intermolecular force field between two water molecules is based on the LJ and Coulomb interactions,

$$u(r) = 4\epsilon_{\alpha\beta} \left[\left(\frac{\sigma_{\alpha\beta}}{r} \right)^{12} - \left(\frac{\sigma_{\alpha\beta}}{r} \right)^6 \right] + \frac{1}{4\pi\epsilon_0} \frac{q_\alpha q_\beta}{r} \quad (2)$$

where r is the distance between sites α and β , q_α is the electric charge of site α , ϵ_0 is the permittivity of vacuum, $\epsilon_{\alpha\beta}$ is the LJ energy scale and $\sigma_{\alpha\beta}$ the repulsive diameter for an $\alpha\beta$ pair. The cross interactions are obtained using the Lorentz-Berthelot mixing rules,

$$\sigma_{\alpha\beta} = \left(\frac{\sigma_{\alpha\alpha} + \sigma_{\beta\beta}}{2} \right); \quad \epsilon_{\alpha\beta} = (\epsilon_{\alpha\alpha}\epsilon_{\beta\beta})^{1/2} \quad (3)$$

The position of site M is $\mathbf{r}_M = \mathbf{r}_O + a(\mathbf{r}_{H_1} - \mathbf{r}_O) + a(\mathbf{r}_{H_2} - \mathbf{r}_O)$ where $a = l_{OM}/[2r_{OH}\cos(\theta/2)]$ for rigid molecules. The force of site M is distributed among the other atoms according to: $\mathbf{F}(H_1) = a\mathbf{F}(M)$, $\mathbf{F}(O) = (1 - 2a)\mathbf{F}(M)$ and $\mathbf{F}(H_2) = a\mathbf{F}(M)$. In the flexible model the average of the r_{OH} distance is used to calculate l_{OM} .

The parameters used in the water models given in table 1. The calculus does not consider the nuclear quantum effects and intermolecular zero-point energy quantum fluctuations.^{31,32} It is known that the above affects the structure and dynamics of the hydrogen-bonding

structure in liquid water via tunneling and proton delocalization.

Table 1

model	k_b kJ/ mol \AA^2	$r_{OH_{eq}}$ \AA	k_a kJ/ mol rad^2	Θ_{eq} deg	d_{OM}^{rel}	ϵ_{OO} /kB	σ_{OO} \AA	q_O e	q_H e
FBA/ ϵ	3000	1.0270	383	114.70	-	95.29998	3.17760	-0.845	0.42250
TIP4P/ ϵ	-	0.9572	-	104.52	0.1050	93.00000	3.16500	0	0.52700
TIP4P/ ϵ_{Flex}	1570	0.9300	212	111.50	0.0830	95.50000	3.17340	0	0.51000
OPC	-	0.8724	-	103.60	0.1594	107.09165	3.16655	0	0.67910
TIP4P-FB	-	0.9572	-	104.52	0.1052	90.12268	3.16555	0	0.52587
TIP4P-ST	-	0.9572	-	104.52	0.0989	89.04258	3.16610	0	0.52172

Notice that $r_{OH_{eq}}$ and Θ_{eq} define the rigid geometry of non-polarizable force fields
The charge on site M is $q_M = -2q_H$

Search of parameters

Using the dipole moment of minimum density method ($\mu_{min\rho}$),⁷ obtains the best geometry that be able to reproduce properties described in table 3.

To acquire the best parameters using the $\mu_{min\rho}$ method, in the case of the TIP4P/ ϵ_{Flex} is linked to obtaining the values of the harmonic potential constants, which reproduce values close to those reported experimentally for the IR spectrum.

The value of the harmonic potential constants (bond and angle) are referred to the reproduction of the experimental values of OH stretching and HOH bending mainly, the parameters calculated for flexible water models given in table 2.

Table 2: Wavenumbers (in cm^{-1}) at the peak of the bands of the power spectrum for the flexible models at liquid phase.

	SPC/Fw ^{22,30}	FAB/ ϵ ³⁰	TIP4P/ ϵ_{Flex}	TIP4P/05f ²⁷	Exp. ²⁷
Cage vibrations	50	50	50	50	50
Intermolecular stretch	278	278	263	230	183.4
Librations A2, B2	513	542	548	570	430, 650
Bending (H–O–H)	1500	1600	1324	1670	1643.5
Stretching (O–H)	3685	3000	2200	3370	3404

The location of the infrared spectrum of the OH stretching is 27% off and the location

due to the HOH bending is 19% off. No greater precision could be achieved because when applying the $\mu_{min\rho}$ method with greater accuracy in this location, it is not possible to have an optimal $\mu_{min\rho}$ value.

The dipole moment of minimum density that could be found with the aforementioned level of error and improves the rigid non-polarizable model (TIP4P/ ϵ) is presented in the figure 1. The $\mu_{min\rho}$ of TIP4P/ ϵ_{Flex} is located at 0.9786 g cm^{-3} , which is located below that obtained by the TIP4P/ ϵ . This gives the final data of the parameterization and the calculations are continued under various thermodynamic conditions to verify the correct parameterization.

Even though the TIP4P/05f model reproduces the correct IR spectrum, it does not compare in this work with the new model and the non-polarizable ones, because it reproduces them with less accuracy than the TIP4P/05 model.²⁷

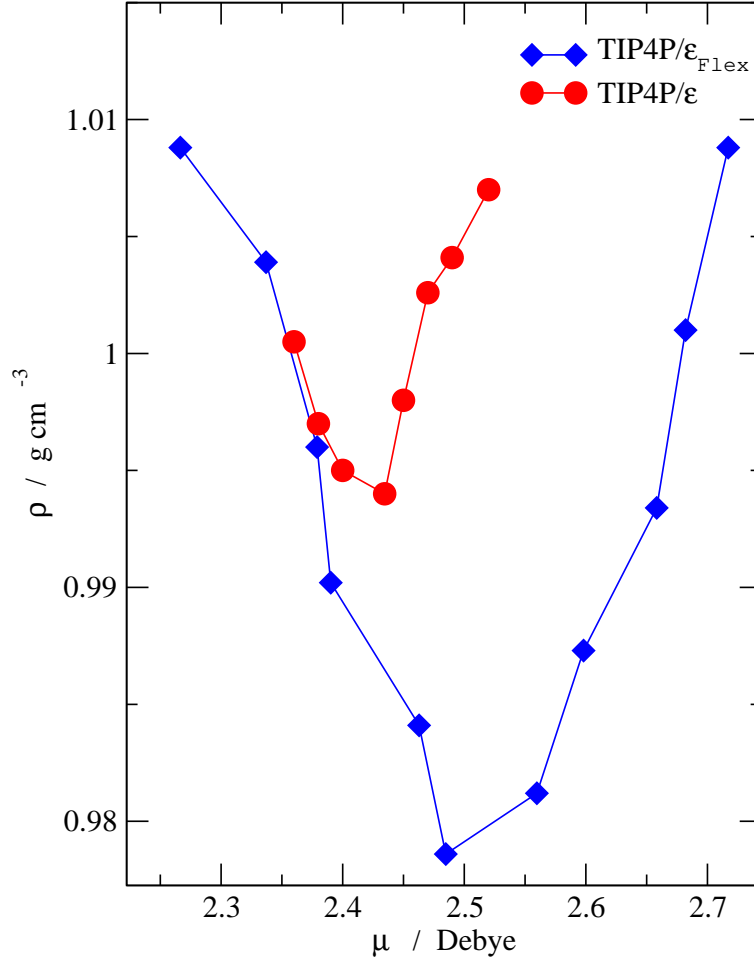


Figure 1: Dipole moment of minimum density $\mu_{min\rho}$ versus density for TIP4P/ ϵ_{Flex} (blue diamonds) and TIP4P/ ϵ (red circles).

Simulation Details

All results of all models here presented, have been calculated with the same level of theory, parameters, and programs in the molecular dynamics simulations.

In this work have been performed molecular dynamics simulations in the isothermal-isobaric ensemble, NPT, with isotropic fluctuations of volume, to compute the liquid properties at different temperatures and pressures, 1 *bar*; these simulations involved typically 500 molecules.

To compute the surface tension has been used the constant volume and temperature ensemble, NVT, and 5832 molecules. To obtain the liquid-vapor interface by setting up a liquid slab surrounded by vacuum in a simulation box with periodic boundary conditions in the three spatial directions. The dimensions of the simulation cell were $Lx = Ly = 46.68$ Å with $Lz = 3Lx$, with z being the normal direction to the liquid-vapor interface. The GROMACS 2016 package^{33,34} was employed in all simulations presented in this work. The equations of motion were solved using the leapfrog algorithm with a time step of 1 *fs* for flexible models and 2 *fs* for non-polarizable rigid models. The temperature was coupled to the Nosé-Hoover thermostat with a parameter $\tau_T = 0.6$ *ps* while the pressure was coupled to the Parrinello-Rahman barostat³⁵ with a coupling parameter $\tau_P = 0.5$ *ps*.

To compute the electrostatic interactions with the particle mesh Ewald approach³⁶ with a grid spacing of 1.2 Å and spline interpolation of order 4. In the isotropic NPT simulations, the real part of the Ewald summation and the LJ interactions were truncated at 9 Å. Long range corrections for the LJ energy and pressure were included. The dielectric constant is obtained from the analysis of the dipole moment fluctuations of the simulation system.^{37,38} The density (ρ), self-diffusion coefficient (D), isothermal compressibility (κ), enthalpy of vaporization ΔH_{vap} , thermal expansion coefficient(α), specific heat capacity C_P , and the dielectric constant (ϵ) were calculated from the same simulation for at least 100 *ns* after an equilibration period of 10 *ns*. For the surface tension computations in the NVT ensemble, the cutoff was set to 26 Å, since the surface tension depends on the truncation

of the interactions³⁹ and the interface cross-sectional area.^{40,41} The equilibration period for the interfacial simulations was 2 *ns*, and the results for the average properties were obtained over an additional 10 *ns* trajectory.

For the calculation of the density of the solid phases here reported (ice Ih), have been carried out isothermal-isobaric (NpT) simulations. For the initial configurations, we used the structural data obtained from diffraction experiments. The NpT simulations are performed under periodical boundary conditions at 1fs and 2fs without seeing any change in density at 10ns. The Berendsen thermostat and barostat were used with parameters of 0.2ps and 0.5ps, respectively

The Berensend barostat was employed for the calculation of the melting temperature and of the density of the ice. The use of this barostat allows the simulation box to expand or contract, and then to form ice or liquid phases. For studying the ice phase and the melting properties, the temperature was fixed with a Berendsen thermostat with a relaxation time of 0.2 *ps*.⁴² For the description of the coexistence between liquid and solid water, have been employed an orthogonal cell. This approach is consistent with the crystallography data of the solid phase Ih.⁴³ The cell size is $Lx = 21.6\text{\AA}$, $Ly = 23.3\text{\AA}$ and $Lz = 53.8\text{\AA}$. Which gives us a contact area between the $Lx * Ly = 503.28\text{\AA}^2$ phases.

Results

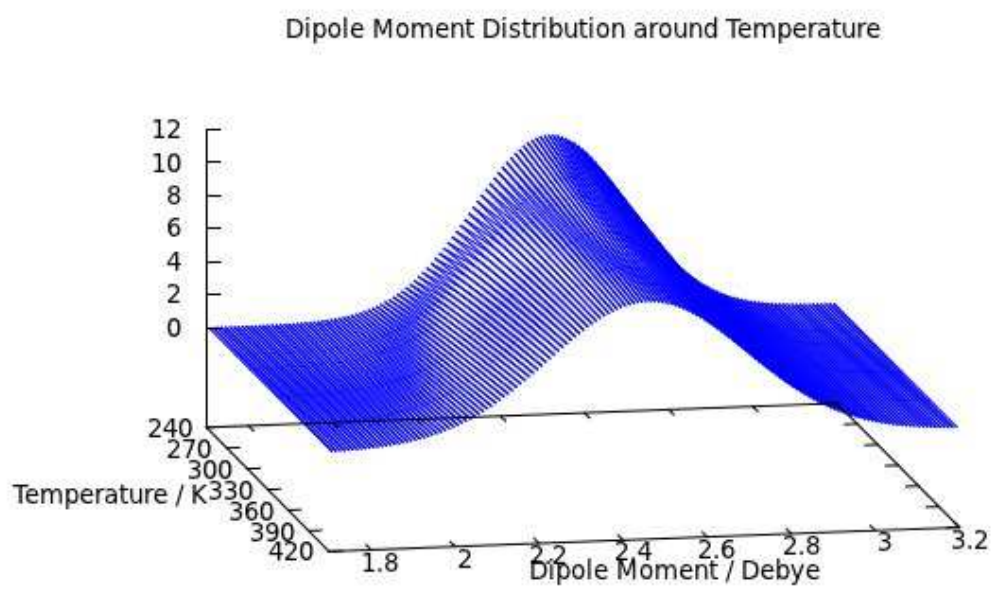


Figure 2: Distribution of molecular dipole moment μ versus 240K to 420K temperatures

Figure 2 represent the distribution of the dipole moment DM of water calculated with the TIP4P/ ϵ_{Flex} in the liquid phase at different temperatures, at low temperatures the DM is closed to 2.5 debyes, the distribution is narrower and the mean value is larger; when the temperature increase the DM decrease to 2.43 debyes, the distribution is more homogeneous and the mean value is smaller

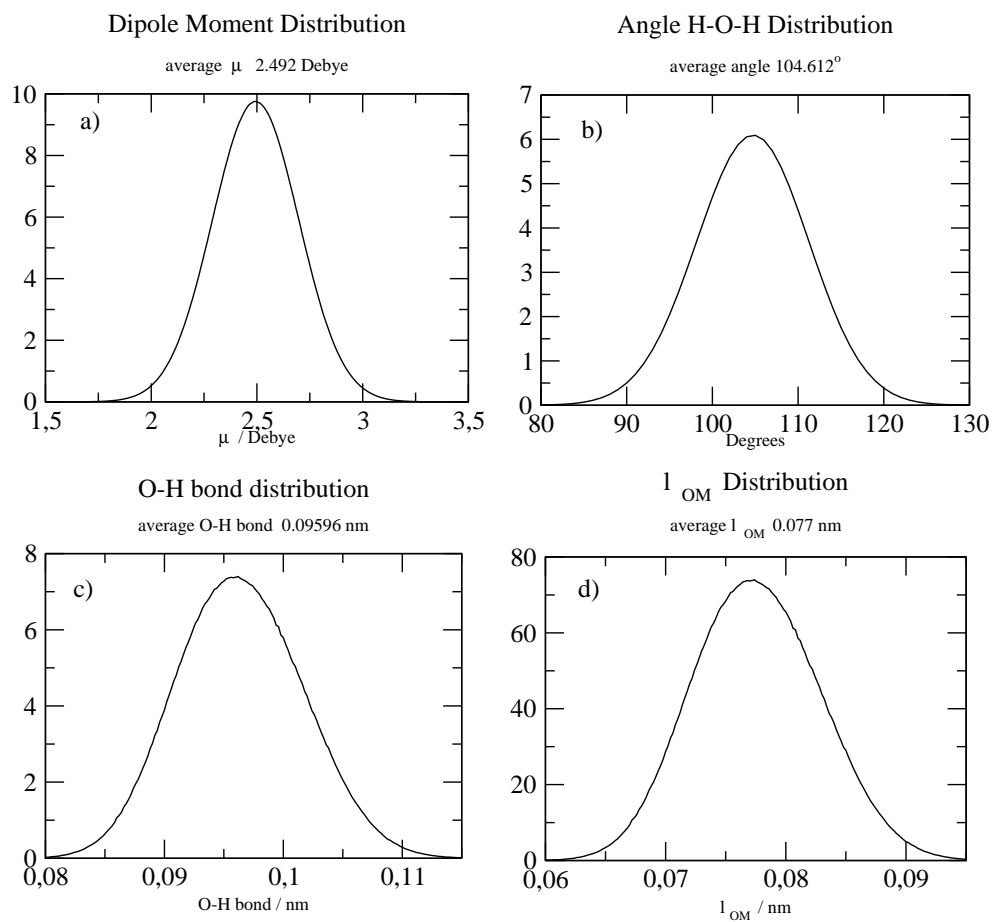


Figure 3: Distributions of flexible models of water:TIP4P/ ϵ_{Flex} at 298 K and 1 bar of temperature and pressure respectively, a) bond distance O-H. b) bending angle HOH. c) molecular dipole moment μ . d) l_{OM} distance.

The water structure of TIP4P/ ϵ_{Flex} at 298 K and 1 bar of temperature and pressure respectively is present in figure 3. Figure 3(a) shows the distribution of dipole moments of the water molecules with an average of 2.492 D, whereas the corresponding experimental value is the 2.42 D. Differently from the non-polarizable rigid models, the TIP4P/ ϵ_{Flex} exhibits a distribution of HOH angles illustrated in figure 3(b), the average angle, 104.612° is close to the average experimental value⁴⁴ which is 106° . The distribution of O-H bond distances for the TIP4P/ ϵ_{Flex} model is illustrated in the figure 3(c), this result shows the average bond distance at 0.09596 nm what is 3% lower than the neutron diffraction value, 0.099 nm ,⁴⁵ and only 2.4% lower than the X-ray diffraction value, 0.09724 nm .^{46,47} The distribution of site M around the bisector of molecule respect to the Oxigen l_{OM} for the TIP4P/ ϵ_{Flex} model is illustrated in figure 3(d), this result shows the average bond distance at of 0.077 nm 27% less than the value of TIP4P/ ϵ . In principle, rigid models can be constructed to give this bond distance, however, they can not adapt to the thermodynamics conditions and can change with the temperature or pressure the O-H bond distance observed both in the experiments and in TIP4P/ ϵ_{Flex} .

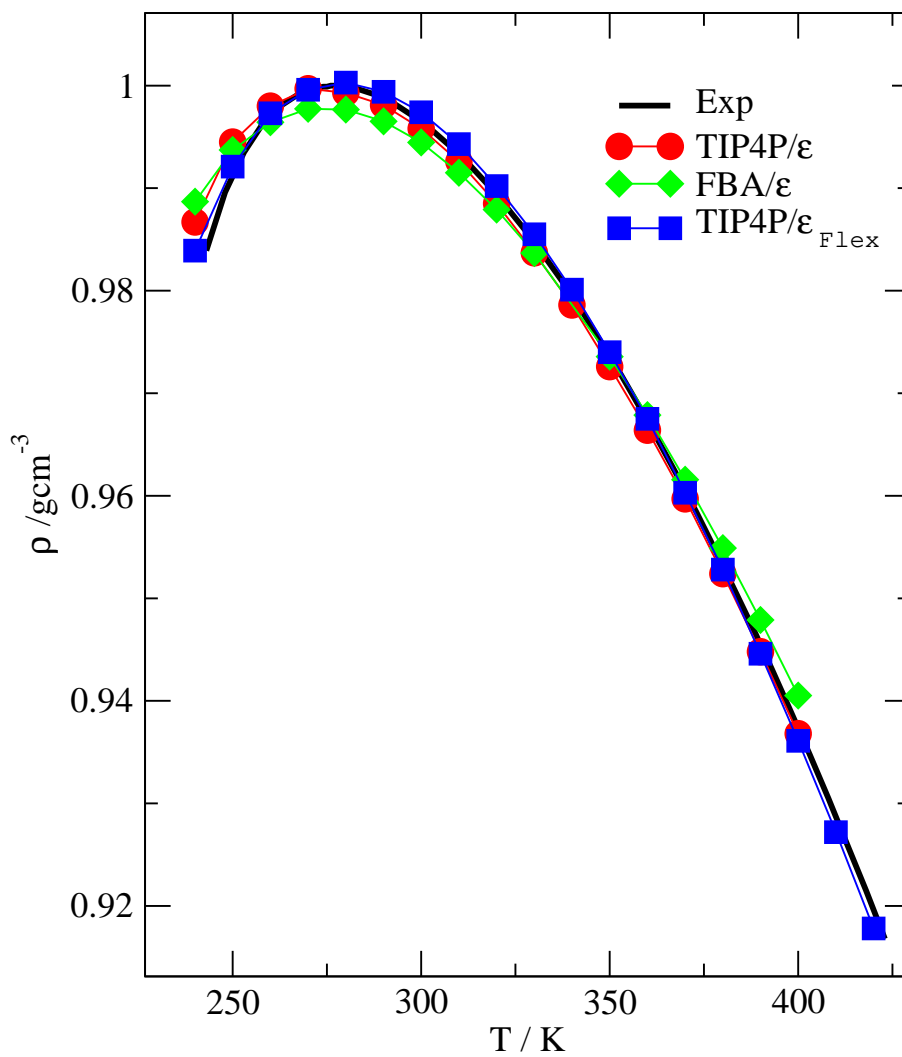


Figure 4: Density as a function of temperature at 1 bar of pressure for the TIP4P/ ϵ_{Flex} (blue squares), FBA/ ϵ (green diamonds) and TIP4P/ ϵ (red circles) models and experimental data⁴⁸ (solid line).

The liquid densities as a function of temperature and 1 bar are shown in Figure 4 for the TIP4P/ ϵ_{Flex} , FBA/ ϵ and TIP4P/ ϵ water models. All the simulation details are the same; the difference is the value of the force fields. The three models, shown in figure 4, give the same ρ -T shape and around the same TMD. The experimental results for temperatures below 273 K are for the metastable liquid. Error concerning the experimental value of the TIP4P/ ϵ_{Flex} model is less than 0.5% in the liquid phase, as expressed in table 3.

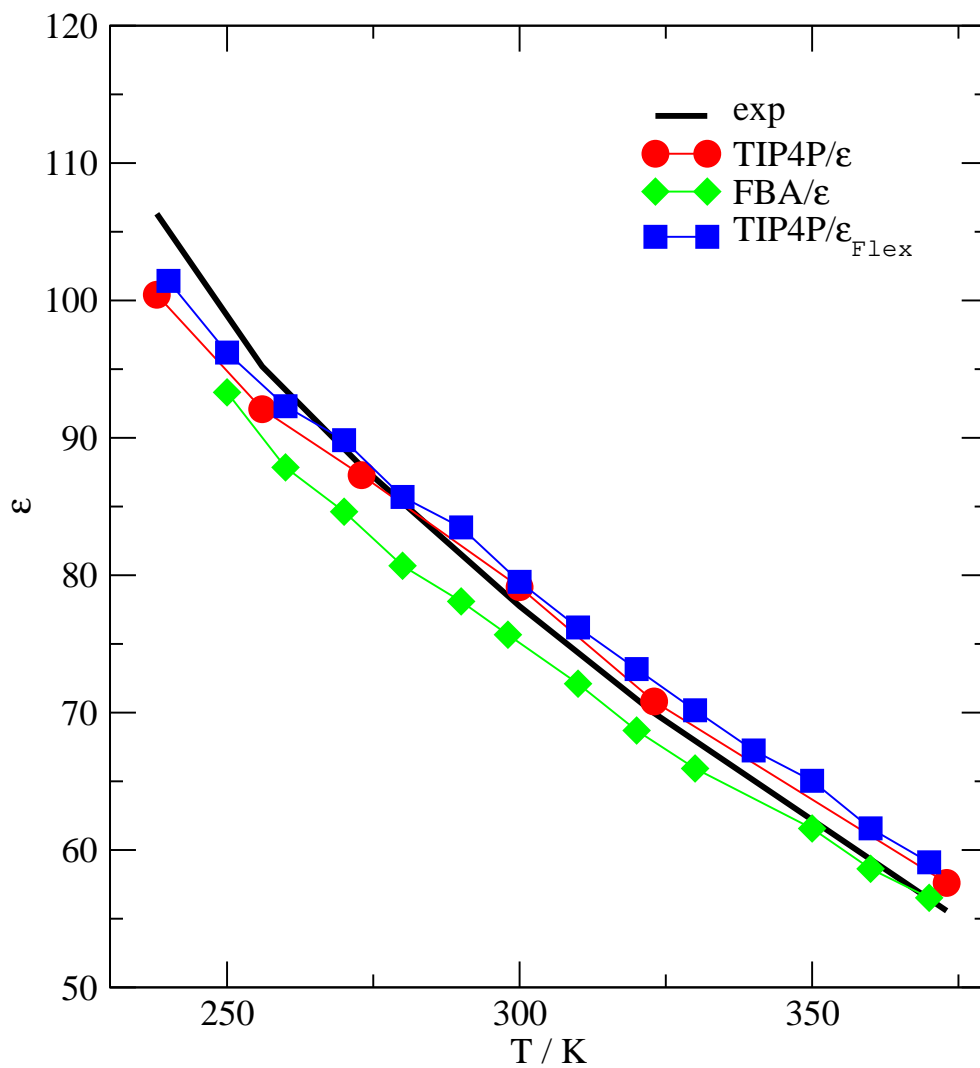


Figure 5: Dielectric constant versus temperature at 1 bar of pressure for the TIP4P/ ϵ_{Flex} (blue squares), FBA/ ϵ (green diamonds) and TIP4P/ ϵ (red circles) models and experimental data⁴⁸ (solid line).

The proper evaluation of the dielectric constant needs long simulations to have the average dipole moment of the system around zero. The dielectric constant results are shown in figure 5 at different temperatures and 1 bar of pressure, as the TIP4P/ ϵ the new model TIP4P/ ϵ_{Flex} reproduce the experimental values with less error than others models.¹⁰ The water static dielectric constant, ϵ , is a collective property of an ensemble of water dipoles, which can be calculated from the equilibrium total dipole moment fluctuations, ($\langle \mathbf{M}^2 \rangle - \langle \mathbf{M} \rangle^2$). The calculations of the dielectric constant was obtained by the equation 4³⁸ of the total dipole moment \mathbf{M} ,

$$\epsilon = 1 + \frac{4\pi}{3k_B T V} (\langle \mathbf{M}^2 \rangle - \langle \mathbf{M} \rangle^2) \quad (4)$$

where k_B is the Boltzmann constant, T is the absolute temperature and V is the volume.

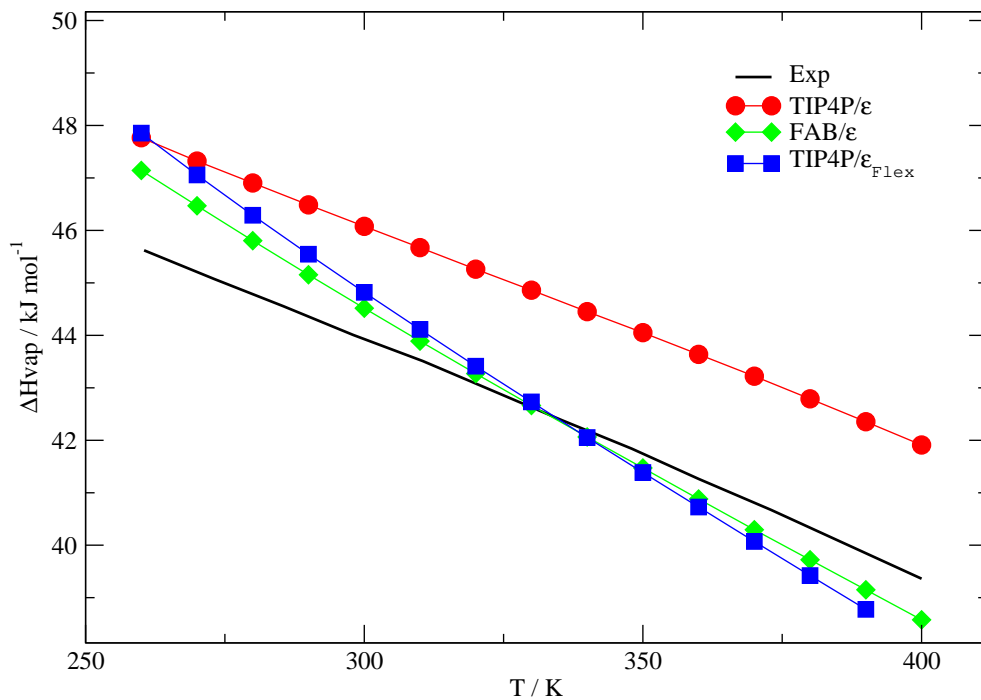


Figure 6: Heat of vaporization ΔH_{vap} as a function of temperature at pressure constant of 1bar for the TIP4P/ ϵ_{Flex} (blue squares), FAB/ ϵ (green diamonds) and TIP4P/ ϵ (red circles) models and experimental data⁴⁸ (solid line).

A wide exploration of the properties behavior which is not linked with the parametrization procedure is necessary when a new model is presented. If the model would be robust, even response functions of property of water would be reproducible, functions exhibit a very peculiar behavior in water, and is important to include most of them.

Figure 6 compares the heat of vaporization, ΔH_{vap} , as a function of the temperature at 1 *bar* for the TIP4P/ ϵ_{Flex} , FBA/ ϵ and TIP4P/ ϵ water models. It shows that flexible FBA/ ϵ and TIP4P/ ϵ_{Flex} agree with the data in a range of 298 K to 365 K with an error less than 2%, which indicates that this type of model does not need any correction. So the comparison with the non-polarizable models will be without correction, table 3 and 4 in this work. The flexibility keeps the correct reproduction for the vapor heat specifically but might affect coexistence properties.

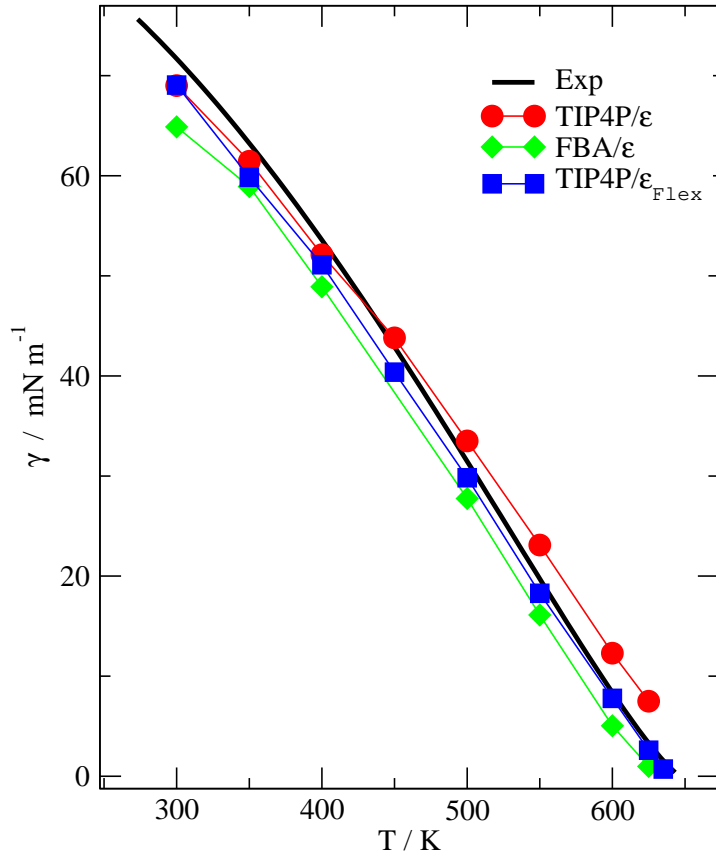


Figure 7: Surface tension as a function of temperature for the TIP4P/ ϵ_{Flex} (blue squares), FBA/ ϵ (green diamonds) and TIP4P/ ϵ (red circles) models and experimental data⁴⁸ (solid line).

The corresponding surface tension γ on the planar interface was calculated from the mechanical definition of γ .⁴⁹

$$\gamma = 0.5L_z[\langle P_{zz} \rangle - 0.5(\langle P_{xx} \rangle + \langle P_{yy} \rangle)] \quad (5)$$

where L_z is the length of the simulation cell in the longest direction and $P_{\alpha\alpha}$ are the diagonal components of the pressure tensor. The factor 0.5 outside the squared brackets take into account the two symmetrical interfaces in the system. The surface tension⁴⁹ results are shown in Figure 7. The results for the TIP4P/ ϵ_{Flex} are in good agreement with experimental data⁴⁸ at all temperatures and improved in high temperatures the TIP4P's results table 3,4.

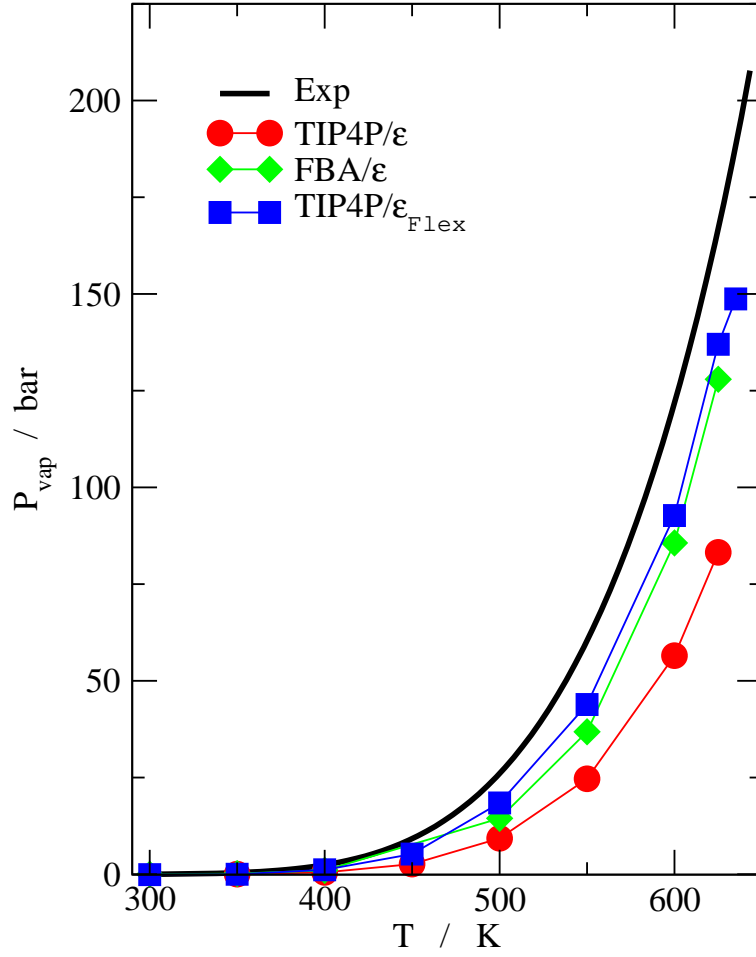


Figure 8: Vapor pressure as a function of temperature for the TIP4P/ ϵ_{Flex} (blue squares), FBA/ ϵ (green diamonds) and TIP4P/ ϵ (red circles) models and experimental data⁴⁸ (solid line).

The P_{vap} increases logarithmically as the temperature increases and models of 3 and 4 sites rigid non-polarizables can not reproduce this behavior, having great differences with respect to the experimental value, see table 3, 4. The FAB ϵ model is a little bit closer to the reproduction of the experimental value,³⁰ however the new TIP4P/ ϵ_{Flex} model achieves a better reproduction; getting to be counted in the table 3. Although the reproduction of this value still fails in all models, the new model is the one that would most be reproduced without compromising the reproduction of the other experimental data.

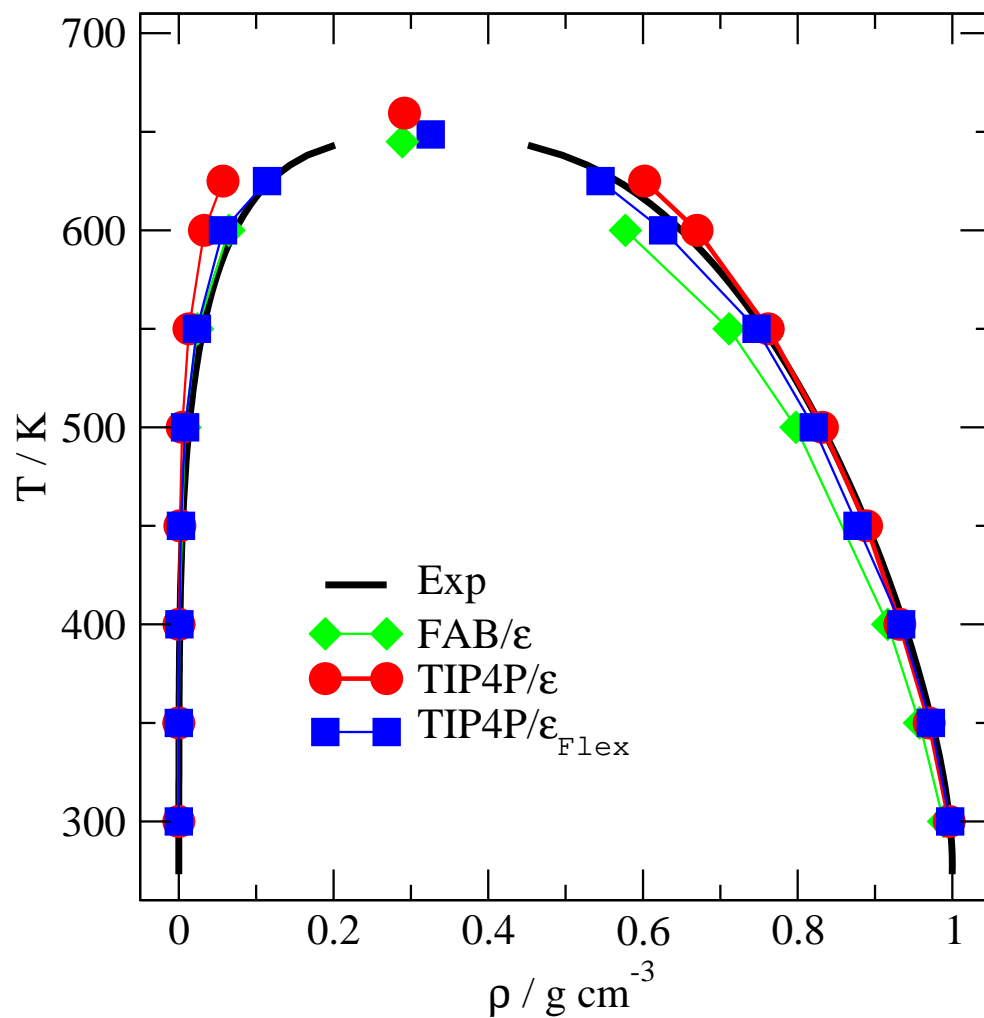


Figure 9: Temperature versus density phase diagram for the the TIP4P/ ϵ_{Flex} (blue squares), FAB/ ϵ (green diamonds) and TIP4P/ ϵ (red circles) models and experimental data⁴⁸ (solid line).

The liquid and vapor densities in simulations of the interface are obtained by fitting the average density profile to a hyperbolic tangent function.⁴⁹ The results shown in figure 9 and given in table 3. The liquid densities predicted by the TIP4P/ ϵ_{Flex} model are in excellent agreement with experimental data⁴⁸ at all temperatures.

The model TIP4P/ ϵ_{Flex} and FBA/ ϵ give vapor densities close to experiments for all temperatures and their predicted critical temperatures are 0.24% closer and 3.06% smaller than experimental data, respectively. The critical parameters for the TIP4P/ ϵ_{Flex} model are $\rho_C = 0.32562 \text{ g cm}^{-3}$ and $T_C=648.66\text{K}$ and they were obtained by using the rectilinear diameters law with critical exponents $\beta= 0.325$.

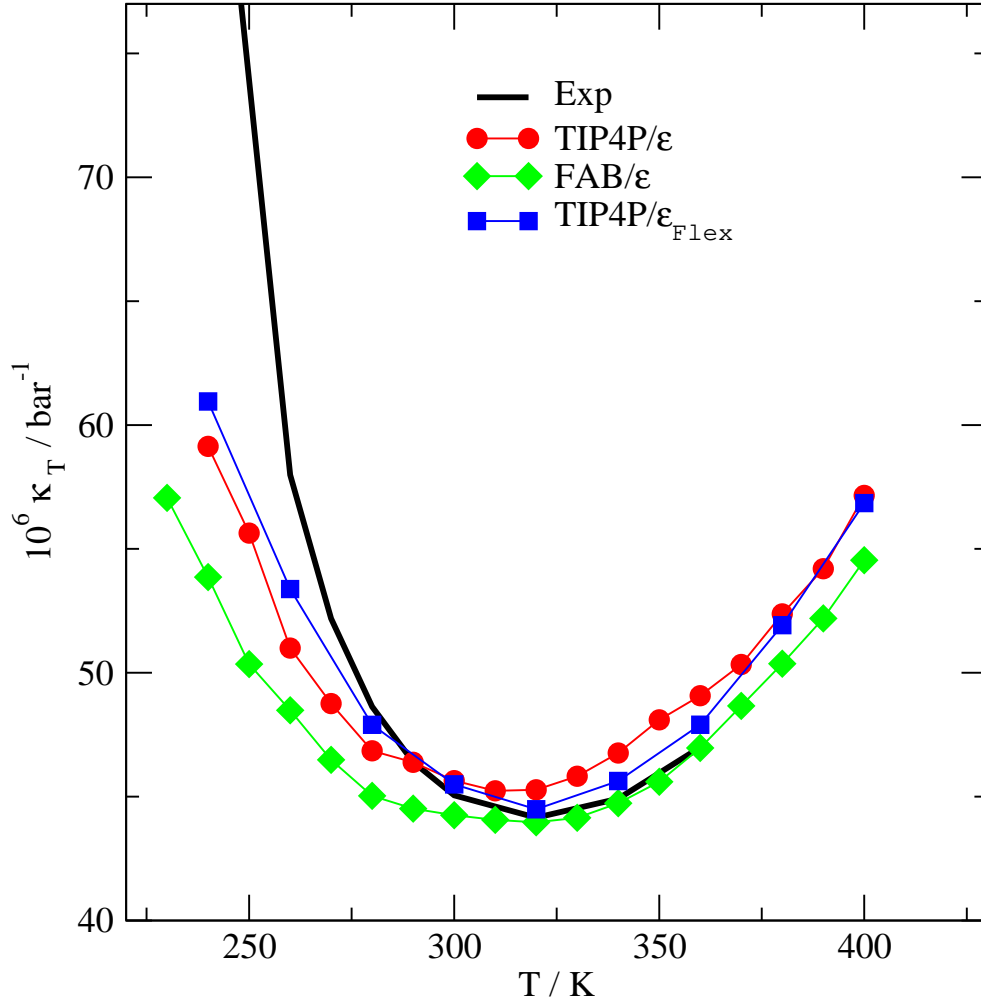


Figure 10: Temperature versus isothermal compressibility (κ) for the the TIP4P/ ϵ_{Flex} (blue squares), FBA/ ϵ (green diamonds) and TIP4P/ ϵ (red circles) models and experimental data⁴⁸ (solid line).

The values of κ_T were obtained from simulations on the isothermal-isobaric ensemble, using

$$\kappa_T = -\frac{1}{V} \left(\frac{\partial V}{\partial P} \right)_T = \frac{1}{\rho} \left(\frac{\partial \rho}{\partial P} \right)_T \quad (6)$$

Simulations of systems containing 500 molecules are performed at 9 different temperatures: $T = 240$ K, 260 K, 280 K, 300 K, 320 K, 340 K, 360 K, 380 K and 400 K. At each temperature, the pressure is varied from $P = 1$ bar to $P = 1200$ bars. The density as a function of pressure is fitted with a cubic polynomial at each temperature and the value of κ_T at $P = 1$ bar is determined from the respective polynomial. The results are given in table 3,3 and in figure 10. The TIP4P/ ϵ_{Flex} model gives a minimum value of κ_T at the same position of experimental data. In general TIP4P/ ϵ_{Flex} model gives results closer to experiment than the TIP4P/ ϵ and FBA/ ϵ .

It is obtained from the Einstein equation

$$D = \lim_{t \rightarrow \infty} \frac{1}{6t} \langle |\mathbf{R}_i(t) - \mathbf{R}_i(0)|^2 \rangle, \quad (7)$$

where $\mathbf{R}_i(t)$ is the center of mass position of molecule i at time t and $\langle \dots \rangle$ denotes time average.

The diffusion coefficient of TIP4P/ ϵ_{Flex} is shown as a function of the temperature in figure 11 and given in table 3, as well as the non-polarizable rigid water models.

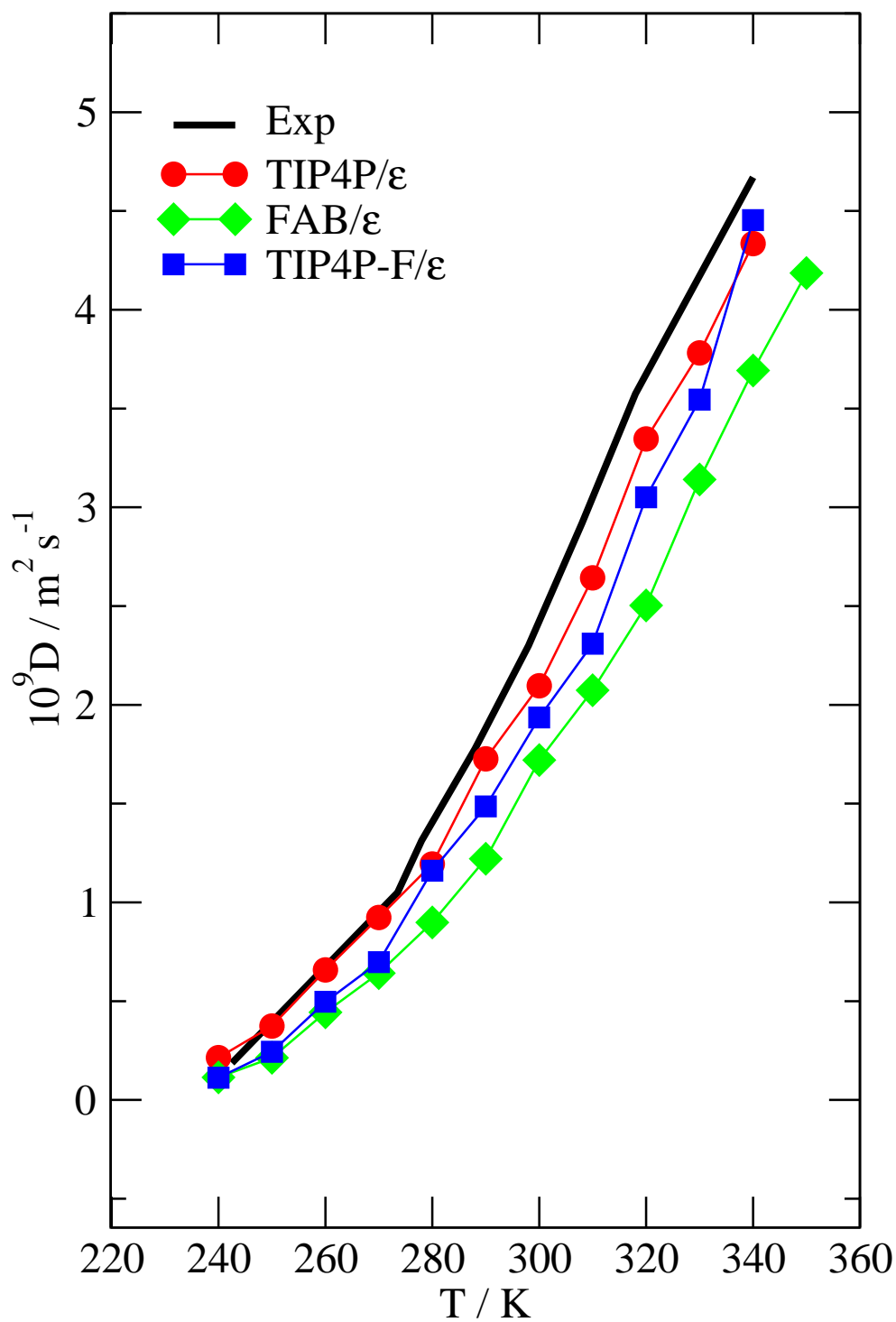


Figure 11: Temperature versus self-diffusion coefficient (D) for the the TIP4P/ ϵ_{Flex} (blue squares), FBA/ ϵ (green diamonds) and TIP4P/ ϵ (red circles) models and experimental data⁴⁸ (solid line).

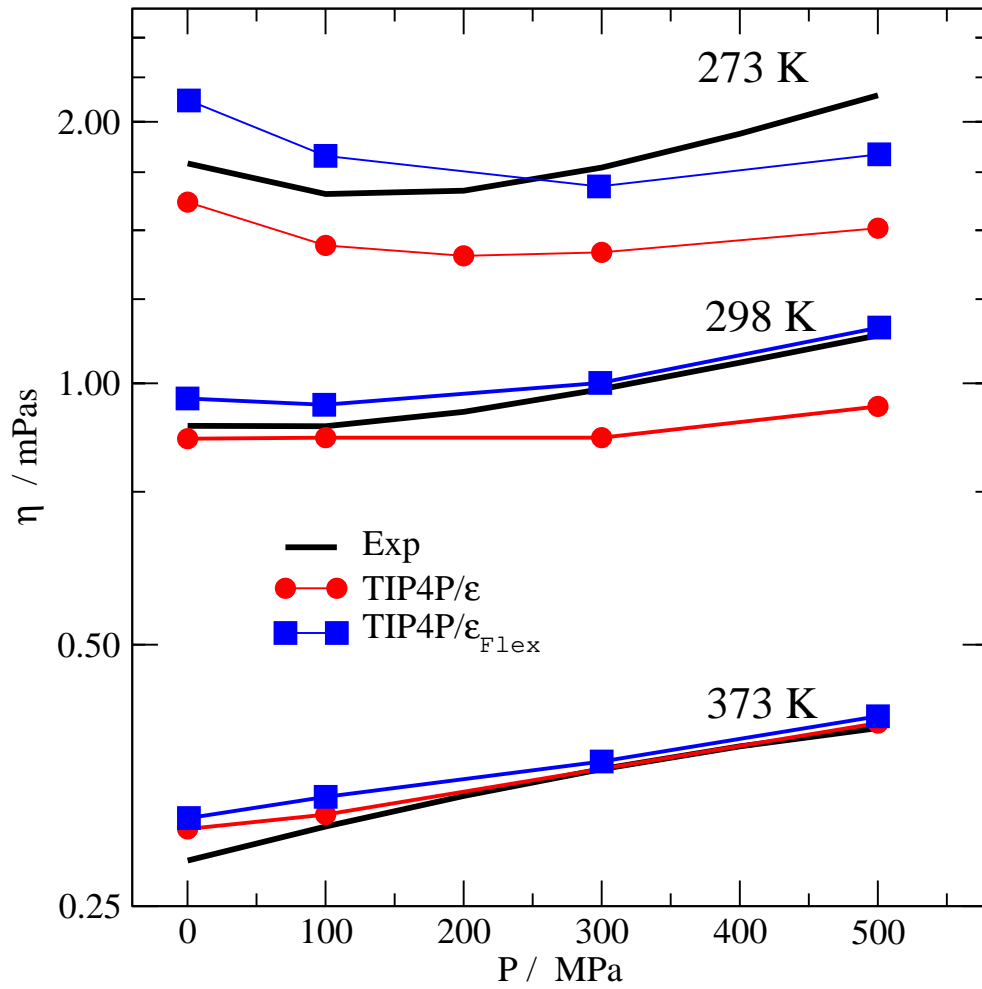


Figure 12: Temperature versus shear viscosity (η) for the the TIP4P/ ϵ_{Flex} (blue squares) and TIP4P/ ϵ (red circles) models and experimental data⁴⁸ (solid line).

The shear viscosity was obtained in this work for all models in tables 3 and 4, NPT simulations are performed for at least 20 million steps with a time step of 1 fs.⁵⁰ The pressure components are saved on a disk every 1 fs, and all the configurations are used as a time origin. The upper limit in the integrations is 8 ps in all cases. The results are shown in figure 12 for The TIP4P/ ϵ_{Flex} and TIP4P/ ϵ at different temperatures and pressures and in tables 3 and 4 for the rest of the models considered. The TIP4P/ ϵ_{Flex} and TIP4P/ ϵ give the same values, within the simulation error at 373K. But at 273 K, the simulation values are systematically lower for all pressures for TIP4P/ ϵ ; at 298K gives the same values at lower pressures but the difference is larger at high pressures. Both models predict the minimum value of shear viscosity at 273 K and 298K.

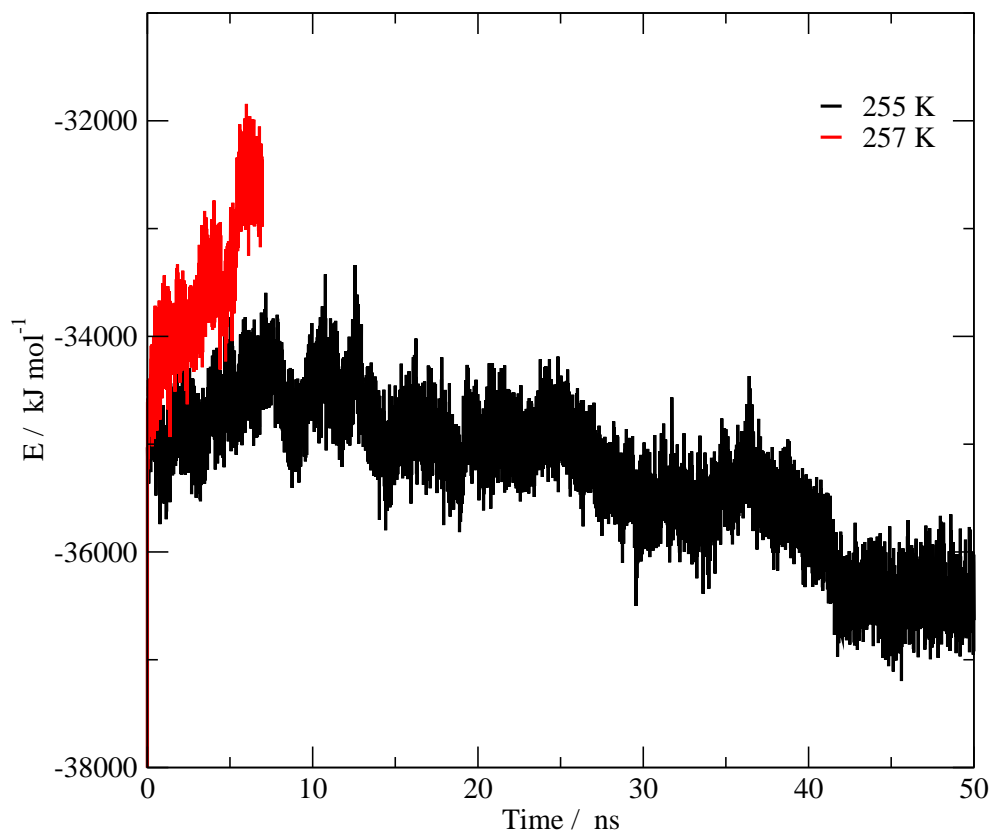


Figure 13: Total energy of a water system vs time, between liquid water in contact with ice Ih for the TIP4P/ ϵ_{Flex} model. The results are NpT simulation runs at 1 bar and $T = 250$ K and 252 K.

The TIP4P/ ϵ_{Flex} force field reproduces the melting temperature, T_m with a difference of 6.59% with respect to the experimental data. Figure13, the red line describes the behavior of the total energy of the system when it turns into a liquid phase and the black line has an energetic decrease that indicates that there is an entire Ice Ih-transforming system. The result of T_m is estimated to be 255.5 K figure13. This result improved the value of TIP4P/ ϵ in 15.5 degrees of temperature.

To calculate this property using direct coexistence simulations.⁵¹ Anisotropic NPT simulations, starting from the same initial configuration, at 1 bar and temperatures ranging from 250 to 260 K with one degree of temperature in each simulation. Simulation was carried out on systems containing 870 water molecules in an elongated simulation cell in the z direction, half in the liquid and half in the ice Ih. The procedure is observing the melting or freezing by inspecting the total energy, if the system is above the T_m the ice region will melt, but if the water is at a temperature below the melting point the liquid water will be ice Ih.⁵¹

In table 3 and 4 compared the most successful model of 3 and 4 sites with respect to the experimental data that can reproduce follow the procedure of Vega et al⁶ for a certain property the prediction of a given water model adopts the value X, and the experimental value is X_{exp} . The score is calculated by the equation (4.8)

$$M = \min \left\{ \text{anint} \left[10 - \text{abs} \left(\frac{X - X_{exp}}{X_{exp} \text{tol}} \right) \right], 0 \right\}, \quad (8)$$

where the tolerance *tol* is given as a percentage and *anint* is the nearest integer function.

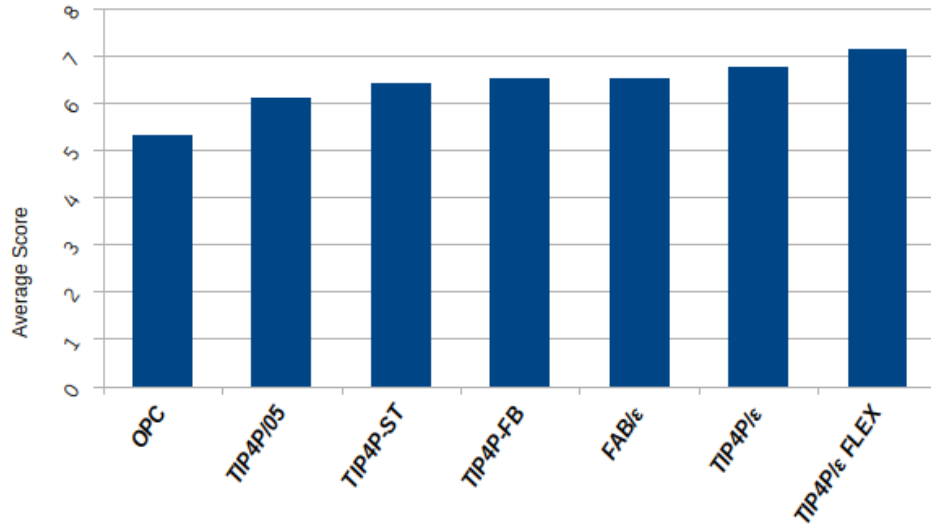


Figure 14: Overall score (out of 10)

Table 3: Experimental and simulation data of TIP4P/05, TIP4P/ ϵ , FAB/ ϵ , TIP4P/ ϵ_{Flex} , water models. Thermodynamic conditions as reported in each entry.

Property	Exp. data	TIP4P/05	TIP4P/ ϵ	FAB/ ϵ	TIP4P/ ϵ_{Flex}	Tol. (%)	TIP4P/05 score	TIP4P/ ϵ score	FAB/ ϵ score	TIP4P/ ϵ_{Flex} score
Enthalpy of phase change / kcal mol ⁻¹										
ΔH_{melt}	1.44	1.16	1.22	0.882	1.799	5	6.1	6.9	2.3	5.0
ΔH_{vap}	10.52	11.99	11.08	10.74	10.84	5	7.2	8.9	9.6	9.4
Critical point properties										
T_C/K	647.1	640	659.5	627.28	648.66	1	8.9	8.1	6.9	9.8
$\rho_C/g\text{ cm}^{-3}$	0.322	0.31	0.29512	0.2854	0.32567	1	6.3	1.7	0.0	8.9
Surface tension/mN m ⁻¹										
γ_{300K}	71.73	69.09	69.00	64.88	69.05	2.5	8.5	8.5	6.2	8.5
γ_{400K}	53.6	50.60	52.11	48.91	51.10	2.5	7.8	8.9	6.5	8.1
γ_{600K}	8.4	7.63	7.86	5.05	7.78	2.5	6.3	7.4	0.0	7.1
Melting properties										
T_m/K	273.15	252	240	251	256	2.5	6.9	5.1	6.8	7.5
$\rho_{liq}/g\text{ cm}^{-3}$	0.999	0.993	0.997	0.9946	0.989784	0.5	8.8	9.6	9.1	8.2
$\rho_{sol}/g\text{ cm}^{-3}$	0.917	0.921	0.929	0.93	0.942507	0.5	9.1	7.4	7.2	4.4
Orthobaric densities and temperature of maximum density TMD										
TMD/K	277	278	277	275.4	277	1	9.6	10.0	9.4	10.0
$\rho_{260K}/g\text{ cm}^{-3}$	0.9969	0.9970	0.9980	0.9964	0.9973	0.5	10.0	9.8	9.9	9.9
$\rho_{298K}/g\text{ cm}^{-3}$	0.9970	0.9930	0.9963	0.9949	0.9970	0.5	9.2	9.9	9.6	10.0
$\rho_{400K}/g\text{ cm}^{-3}$	0.9375	0.9300	0.9368	0.9405	0.9361	0.5	8.4	9.9	9.4	9.7
$\rho_{450K}/g\text{ cm}^{-3}$	0.8903	0.8790	0.8842	0.8982	0.8801	0.5	7.5	8.6	8.2	7.7
Isothermal compressibility / 10 ⁻⁶ bar ⁻¹)										
κ_T [1 bar; 298 K]	45.3	46.85	45.77	44.29	45.7	1	6.6	9.0	7.8	9.1
κ_T [1 bar; 318 K]	44.25	46.46	45.25	43.97	44.58	1	5.0	7.7	9.4	9.3
κ_T [1 bar; 360 K]	47	50.17	49.01	46.89	47.901	1	3.3	5.7	9.8	8.1
Thermal expansion coefficient / 10 ⁵ K ⁻¹)										
α_P [1 bar; 298 K]	22.66	22.6	23.79	29.29	24.55	5	9.9	9.0	4.1	8.3
α_P [1 bar; 350 K]	68.2	69.54	70.87	65.83	65.06	5	9.6	9.2	9.3	9.1
Heat capacity at constant pressure/ cal mol ⁻¹ K ⁻¹										
C_p [liq 298 K; 1 bar]	18	21.10	19.80	25.20	28.00	5	6.6	8.0	2.0	0.0
C_p [ice 250 K; 1 bar]	8.3	14.00	13.90	7.65	21.00	5	0.0	0.0	8.4	0.0
Liquid-vapor phase equilibrium (density) / g cm ⁻³										
ρ_{vap} [500 K]	0.0128	0.006	0.0044	0.0078	0.0082	5	0.0	0.0	2.2	2.8
ρ_{vap} [625 K]	0.1139	0.13	0.057	0.161	0.1141	5	7.2	0.0	1.7	10.0
ρ_{liq} [400 K]	0.9433	0.932	0.932	0.9163	0.9337	5	9.8	9.8	9.4	9.8
ρ_{liq} [500 K]	0.6694	0.821	0.832	0.7977	0.8209	5	5.5	5.1	6.2	5.5
ρ_{liq} [625 K]	0.5764	0.54	0.602	0.489	0.5452	5	8.7	9.1	7.0	8.9
Gas properties / bar										
p_v [450 K]	9.32	4.46	2.64	4.29	5.23	5	0.0	0.0	0.0	1.2
p_v [550 K]	60.48	16.1	24.69	36.83	43.9	5	0.0	0.0	2.2	4.5
Static dielectric constant										
ϵ [liq; 298 K]	78.5	58	79.36	75.65	79.06	1	0.0	8.9	6.4	9.3
ϵ [liq; 350 K]	62.12	43.1	63.51	61.56	64.93	1	0.0	7.8	9.1	5.5
ϵ [10kbar, 300K]	103.63	81.9	103.2	104.9	102.296	1	0.0	9.6	8.8	8.7
T_m -TMD- T_c ratios										
$T_m[I_h]/T_c$	0.422	0.394	0.36	0.40	0.39	5	8.7	7.2	9.0	8.7
TMD/ T_c	0.428	0.434	0.42	0.43	0.42	5	9.7	9.6	9.5	10.0
TMD- T_m (K)	4	26	37	24.4	21	5	0.0	0.0	0.0	0.0
Densities of ice Ih/g cm ⁻³										
ρ [I _h 250 K; 1 bar]	0.92	0.9207	0.922	0.93	0.939	0.5	9.8	9.6	7.8	5.9
ρ [I _h 220 K; 1 bar]	0.923	0.9248	0.926	0.935	0.94	0.5	9.6	9.3	7.4	6.3
ρ [I _h 150 K; 1 bar]	0.969	0.936	0.937	0.974	0.979	0.5	3.2	3.4	9.0	7.9
EOS high pressure										
ρ [373 K; 10 kbar]	1.201	1.204	1.202	1.215	1.1977	0.5	9.5	9.9	7.7	9.5
ρ [373 K; 20 kbar]	1.322	1.321	1.318	1.339	1.3131	0.5	9.8	9.3	7.4	8.7
Self-diffusion coefficient/cm ² s ⁻¹										
$\ln D_{278K}$	-11.24	-11.27	-11.27	-11.58	-11.46	1	9.7	9.7	7.0	8.0
$\ln D_{298K}$	-10.68	-10.79	-10.79	-11.01	-10.908	1	9.0	9.0	6.9	7.9
E_a k _J mol ⁻¹	18.4	16.2	20.51	15.98	19	2	4.0	4.3	3.4	8.4
Shear viscosity / mPa s										
η [1 bar; 298 K]	0.896	0.855	0.855	1.265	0.958	5	9.1	9.1	1.8	8.6
η [1 bar; 373 K]	0.284	0.289	0.289	0.364	0.314	5	9.6	9.6	4.4	7.9
Overall score (out of 10)							6.15	6.81	6.62	7.24

Table 4: Experimental and simulation data of TIP4P-FB, TIP4P-ST and OPC water models. Thermodynamic conditions as reported in each entry.●

Property	Exp. data	TIP4P-FB	TIP4P-ST	OPC	Tol. (%)	TIP4P-FB score	TIP4P-ST score	OPC score
Enthalpy of phase change / kcal mol ⁻¹								
ΔH_{melt}	1.44	1.24	1.24	0.871	5	7.2	7.2	2.1
ΔH_{vap}	10.52	10.9	10.9	11.06	5	9.3	9.3	9.0
Critical point properties								
T_c/K	647.1	658.5	660.5	685	1	8.2	7.9	4.1
$\rho_c/g\text{ cm}^{-3}$	0.322	0.2983	0.2970	0.3019	1	2.7	2.3	3.8
Surface tension/mN m ⁻¹								
γ_{300K}	71.73	67.13	68.98	74.44	2.5	7.4	8.5	8.5
γ_{400K}	53.6	53.76	52.07	58.81	2.5	9.9	8.9	6.1
γ_{600K}	8.4	12.30	11.82	18.78	2.5	0.0	0.0	0.0
Melting properties								
T_m/K	273.15	243	246	242	2.5	5.6	6.0	5.4
$\rho_{liq}/g\text{ cm}^{-3}$	0.999	0.988	0.99	0.894	0.5	7.8	8.2	0.0
$\rho_{sol}/g\text{ cm}^{-3}$	0.917	0.926	0.928	0.994	0.5	8.0	7.6	0.0
Orthobaric densities and temperature of maximum density TMD								
TMD/K	277	281	277	272	1	8.6	10.0	8.2
$\rho_{260K}/g\text{ cm}^{-3}$	0.9969	0.9950	0.9980	1.0000	0.5	9.6	9.8	9.4
$\rho_{298K}/g\text{ cm}^{-3}$	0.9970	0.9958	0.9970	0.9966	0.5	9.8	10.0	9.9
$\rho_{400K}/g\text{ cm}^{-3}$	0.9375	0.9384	0.9396	0.9400	0.5	9.8	9.6	9.5
$\rho_{450K}/g\text{ cm}^{-3}$	0.8903	0.8914	0.8911	0.8984	0.5	9.8	9.8	8.2
Isothermal compressibility / 10 ⁻⁶ bar ⁻¹)								
κ_T [1 bar; 298 K]	45.3	44.8	45.2	47.4	1	8.9	9.8	5.4
κ_T [1 bar; 318 K]	44.25	44.9	45.2	46.6	1	8.5	7.9	4.7
κ_T [1 bar; 360 K]	47	49.4	48.93	48.5	1	4.9	5.9	6.8
Thermal expansion coefficient / 10 ⁵ K ⁻¹)								
α_P [1 bar; 298 K]	22.66	23	24	25.62	5	9.7	8.8	7.4
α_P [1 bar; 350 K]	68.2	61.9	60.3	67.49	5	8.2	7.7	9.8
Heat capacity at constant pressure/ cal mol ⁻¹ K ⁻¹								
C_p [liq 298 K; 1 bar]	18	19.20	18.90	18.00	5	8.7	9.0	10.0
C_p [ice 250 K; 1 bar]	8.3	13.93	14.03	13.81	5	0.0	0.0	0.0
Liquid-vapor phase equilibrium (density) / g cm ⁻³								
ρ_{vap} [500 K]	0.0128	0.005	0.0045	0.0017	5	0.0	0.0	0.0
ρ_{vap} [625 K]	0.1139	0.06059	0.058	0.034	5	0.6	0.2	0.0
ρ_{liq} [400 K]	0.9433	0.938	0.936	0.938	5	9.9	9.8	9.9
ρ_{liq} [500 K]	0.6694	0.831	0.833	0.846	5	5.2	5.1	4.7
ρ_{liq} [625 K]	0.5764	0.597	0.602	0.657	5	9.3	9.1	7.2
Gas properties / bar								
p_v [450 K]	9.32	3.102	2.86374	3.1	5	0.0	0.0	0.0
p_v [550 K]	60.48	25.042	22.30	43.3	5	0.0	0.0	4.3
Static dielectric constant								
ϵ [liq; 298 K]	78.5	76.86	82	79.5	1	7.9	5.5	8.7
ϵ [liq; 350 K]	62.12	62.6	64.3	63.178	1	9.2	6.5	8.3
ϵ [10kbar, 300K]	103.63	100.874	100.596	98.413	1	7.3	7.1	5.0
T_m -TMD- T_c ratios								
$T_m[I_h]/T_c$	0.422	0.36	0.37	0.35	5	7.5	7.7	6.7
TMD/ T_c	0.428	0.42	0.41	0.39	5	9.9	9.6	8.6
TMD- T_m (K)	4	38	31	30	5	0.0	0.0	0.0
Densities of ice Ih/g cm ⁻³								
ρ [I _h 250 K; 1 bar]	0.92	0.925	0.927	0.893	0.5	8.9	8.5	4.1
ρ [I _h 220 K; 1 bar]	0.923	0.929	0.932	0.897	0.5	8.7	8.0	4.4
ρ [I _h 150 K; 1 bar]	0.969	0.939	0.942	0.906	0.5	3.8	4.4	0.0
EOS high pressure								
ρ [373 K; 10 kbar]	1.201	1.205	1.206	1.18777	0.5	9.3	9.2	7.8
ρ [373 K; 20 kbar]	1.322	1.322	1.324	1.29752	0.5	10.0	9.7	6.3
Self-diffusion coefficient/cm ² s ⁻¹								
ln D_{278K}	-11.24	-11.16	-11.25	-11.31	1	9.3	9.9	9.4
ln D_{298K}	-10.68	-10.65	-10.66	-10.8	1	9.7	9.8	8.9
E_a k _J mol ⁻¹	18.4	17.56	20.318	17.56	2	7.7	4.8	7.7
Shear viscosity / mPa s								
η [1 bar; 298 K]	0.896	0.95	0.81	0.815	5	8.8	8.1	8.2
η [1 bar; 373 K]	0.284	0.287	0.283	0.277	5	9.8	9.9	9.5
Overall score (out of 10)						6.6	6.4	5.4

The 4 sites rigid and non-polarizable models of water have been widely studied and reparametrized since the TIP4P was published, achieving improvements of 53% by the TIP4P/05, and reaching an optimization with the TIP4P/ ϵ model and improving only 2.46% with respect to TIP4P/05. In the same timeline, there have been efforts to improve this type of model, such as the TIP4P-FB and OPC models, which as seen in figure 14, the TIP4P-FB improves the TIP4P/05 and is very close to the TIP4P/ ϵ and the OPC that was optimized in the liquid phase, is far from the TIP4P/05 when it is analyzed in a wide and established range of properties in different thermodynamic phases. By improving the 3 sites rigid and non-polarizable models with the FAB/ ϵ model, a parametrization way is established with the IR spectrum as experimental data target and thus be able to add the harmonic potential and improve the reproduction of the experimental data. As seen in table3,4 and in figure 14. The TIP4P/05 model has been improved by FAB/ ϵ an 7.1% with respect to the properties that were already reproduced and the TIP4P/ ϵ_{Flex} improved an 15% and open a new possibility by having flexibility and reproducing various properties with less error.

Table 5: •

Property	Average score (out of 10)						
	TIP4P-FB	TIP4P-ST	OPC	TIP4P/05	TIP4P/ ϵ	FAB/ ϵ	TIP4P/ ϵ_{Flex}
Enthalpy of phase change	8.2	8.2	5.5	6.7	7.9	5.9	7.2
Critical point properties	5.4	5.1	4	7.6	4.9	3.5	9.3
Surface tension	5.8	5.8	4.9	7.5	8.3	4.2	7.9
Melting properties	7.1	7.3	1.8	8.3	7.4	7.7	6.7
Orthobaric densities and TMD	9.5	9.8	9	8.9	9.6	9.3	9.5
Isothermal compressibility	7.4	7.8	5.6	4.9	7.5	9	8.8
Thermal expansion coefficient	8.9	8.3	8.6	9.8	9.1	6.7	8.7
Heat capacity at constant pressure	4.3	4.5	5	3.3	4	5.2	0
Liquid-vapor phase equilibrium (density)	5	4.9	4.4	6.2	4.8	5.3	7.4
Gas properties	0	0	2.2	0	0	1.1	2.9
Static dielectric constant	8.2	6.4	7.3	0	8.8	8.1	7.8
T _m -TMD-T _c ratios	5.8	5.7	5.1	6.1	5.6	6.1	6.2
Densities of ice Ih	7.1	7	2.8	7.5	7.4	8.1	6.7
EOS high pressure	9.7	9.4	7	9.7	9.6	7.5	9.1
Self-diffusion coefficient	8.9	8.2	8.7	7.6	7.7	5.8	8.1
Shear viscosity	9.3	9	8.8	9.4	9.4	3.1	8.3

The table 5 shows the average score of the properties studied with each model and it is notable that those of 4 sites rigid and non-polarizable models have more properties with a score lower than 5 and that the new TIP4P/ ϵ_{Flex} model only has two below 5, which are *Heat capacity at constant pressure C_P and Gas properties P_{vap}* , being one of the challenges for the next reparametrization of a water model or for any different type of model.

conclusions

This work has important implications for the understanding of molecular interactions in water and for the construction of molecular models in general, not only to implement the $\mu_{min\rho}$ method and the IR spectrum as experimental target for harmonic potential parametrization, but to understand the main idea of using the methodology to parameterize. By building a more closer to experimental data, but still approximate model, Understand which microscopic interactions are truly important for describing the properties of interest; for example, one part to highlight from this work is that the Dipole Moment of minimum density method is capable to construct force fields that define the optimal structure and capturing the effect of mutual polarization for a very wide range of water properties. Another interesting part is the role of model parameterization in establishing this understanding. For most practical problems it is impossible to explore the entire parameter space, so we can provide a way to reparameterization of water models and other molecules.

Acknowledgements

The author thank Consejo Nacional de Ciencia y Tecnología (CONACYT) for financial support and acknowledge Centro de Supercómputo of Universidad Autónoma Metropolitana (Yoltla) for allocation of computer time.

References

- (1) R. Fuentes-Azcatl, M.C. Barbosa, Sodium Chloride, NaCl/ ϵ : New Force Field, *J. Phys. Chem. B.* 120 (2016), 2460-2470.
- (2) R. Fuentes-Azcatl, M.C. Barbosa, Potassium bromide, KBr/ ϵ : New Force Field, *Physica A.* 491 (2018) 480-489
- (3) V García-Melgarejo, E Núñez-Rojas, J Alexandre, United atom model via interactions with explicit water (UAMI-EW): Alcohols and ketones, *J. Mol. Liq.* (2020) 114576
- (4) P. S. Georgoulia, N. M. Glykos, Molecular simulation of peptides coming of age: Accurate prediction of folding, dynamics and structures, *Arch. Biochem.*, N.Y. 664 (2019) 76-88
- (5) B. Guillot, A reappraisal of what we have learnt during three decades of computer simulations on water, *J. Molec. Liq.* 101 (2002) 219.
- (6) C. Vega, J. L. F. Abascal, Simulating Water with Rigid Non-Polarizable Models: A General Perspective. *Phys. Chem. Chem. Phys.* 13 (2011) 19663-19688.
- (7) R. Fuentes-Azcatl, J. Alexandre, Non-polarizable force field of water based on the dielectric constant: TIP4P/ ϵ , *Phys. Chem. B* 118 (2014) 1263-1272.
- (8) R. Fuentes-Azcatl, M.C. Barbosa, Thermodynamic and dynamic anomalous behavior in the TIP4P/ ϵ water model, *Physica A.* 444 (2016) 86-94.

- (9) R. Fuentes-Azcatl, N. Mendoza, J. Alejandre, Improved SPC force field of water based on the dielectric constant: SPC/ ϵ , *J. Physica A.* 420 (2015) 116-123.
- (10) P. Zarzycki, G. Benjamin, Temperature-dependence of the dielectric relaxation of water using non-polarizable water models, *Phys. Chem. Chem. Phys.* 22 (2020) 1011.
- (11) W. L. Jorgensen, J. Chandrasekhar, J. D. Madura, R. W. Impey, M. L. Klein, Comparison of simple potential functions for simulating liquid water, *J. Chem. Phys.* 79 (1983) 926-935.
- (12) H. J. C. Berendsen, J. P. M. Postma, W. F. van Gunsteren, J. Hermans, Simple Point Charge Water. In *Intermolecular Forces*, Pullman, B., Ed.; Reidel: Dordrecht, The Netherlands, 1981
- (13) J. L. F. Abascal, C. Vega, A general purpose model for the condensed phases of water: TIP4P/2005, *J. Chem. Phys.* 123 (2005) 234505.
- (14) L. P. Wang, T. J. Martinez and V. S. Pande, Building Force Fields: An Automatic, Systematic, and Reproducible Approach, *J. Phys. Chem. Lett.*, 5 (2014) 1885-1891.
- (15) Y. Qiu, P. S. Nerenberg, T. Head-Gordon, L.P. Wang, Systematic Optimization of Water Models Using Liquid/Vapor Surface Tension Data, *J. Phys. Chem. B*, 123 (2019) 7061-7073
- (16) F. J. Salas, G. A. Méndez-Maldonado, E. Nunez-Rojas, G. E. Aguilar-Pineda, H. Domínguez, J. Alejandre, Systematic procedure to parametrize force fields for molecular fluids. *J. Chem. Theory Comput.* 11 (2015) 683-693.
- (17) D. E. Smith, A. D. J. Haymet, Structure and dynamics of water and aqueous solutions: The role of flexibility, *J. Chem. Phys.* 96 (1992) 8450 .
- (18) I. G. Tironi, R. M. Brunne, W. F. van Gunsteren, Flexible simple point-charge water model with improved liquid-state properties, *Chem. Phys. Lett.* 250 (1996) 19.

- (19) B. S. Gonzalez, E. G. Noya, C. Vega, L. M. Sese, Nuclear quantum effects in water clusters: the role of molecular flexibility, *J. Phys. Chem. B* 114 (2010) 2484.
- (20) I. Kurisaki, T. Takahashi, Assessment of dynamic properties of water around a monovalent ion: a classical molecular dynamics simulation study, *Comput. Theor. Chem.* 966 (2011) 26.
- (21) J. Marti, E. Guardia, J. A. Padro, Dielectric properties and infrared spectra of liquid water: Influence of the dynamic cross correlations, *J. Chem. Phys.* 101 (1994) 10883.
- (22) Y. J. Wu, H. L. Tepper, and G. A. Voth, Flexible simple point-charge water model with improved liquid-state properties, *J. Chem. Phys.* 124 (2006) 024503 .
- (23) O. Teleman, B. Jonsson, and S. Engstrom, A molecular dynamics simulation of a water model with intramolecular degrees of freedom, *Mol. Phys.* 60 (1987) 193.
- (24) J. L. Barrat and I. R. McDonald, The role of molecular flexibility in simulations of water, *Mol. Phys.* 70 (1990) 535.
- (25) A. Wallqvist and O. Teleman, Properties of flexible water models, *Mol. Phys.* 74 (1991) 515.
- (26) H. L. Lemberg, F. H. Stillinger, Central-force model for liquid water, *J. Chem. Phys.* 62 (1975) 1677.
- (27) M. A. González, José L. F. Abascal, A flexible model for water based on TIP4P/2005, *J. Chem. Phys.* 135 (2011) 224516.
- (28) K. Toukan and A. Rahman, Molecular-dynamics study of atomic motions in water, *Phys. Rev. B* 31 (1985) 2643.
- (29) R Fuentes-Azcatl, H Domínguez, Prediction of experimental properties of CO₂: improving actual force fields, *J. Mol. Model.* 25 (2019) 146.

- (30) R. Fuentes-Azcatl, M.C. Barbosa, Flexible bond and angle, FBA/ ϵ model of water, *J. Mol. Liq.* 303 (2020) 112598.
- (31) M. Ceriotti, W. Fang, P. G. Kusalik, R. H. McKenzie, A. Michaelides, M. A. Morales, T. E. Markland, Nuclear Quantum Effects in Water and Aqueous Systems: Experiment, Theory, and Current Challenges *Chem. Rev.*, 116 (2016) 7529-7550.
- (32) F. Paesani, S. Yoo, H. J. Bakker and S. S. Xantheas, Nuclear Quantum Effects in the Reorientation of Water, *J. Phys. Chem. Lett.*, 1 (2010) 2316-2321.
- (33) M. J. Abraham, T. Murtola, R. Schulz, S. Páll, J. C. Smith, B. Hess, E. Lindahl, GROMACS: High performance molecular simulations through multi-level parallelism from lap-tops to supercomputers. *SoftwareX* 1-2 (2015) 19-25.
- (34) D. van der Spoel, E. Lindahl, B. Hess, G. Groenhof, A. E. Mark, H. J. C. Berendsen, GROMACS: Fast, Flexible and Free. *J. Comput. Chem.* 26 (2005) 1701.
- (35) M. Parrinello and A. Rahman, *J. Appl. Phys.* 52 (1981) 7182 .
- (36) U. Essmann, L. Perera, M.L. Berkowitz, T. Darden, H. Lee, L.G. Pedersen, A smooth particle mesh Ewald method, *J. Chem. Phys.* 103 (1995) 8577-8592.
- (37) J.P. Hansen, I.R. McDonald, *Theory of Simple Liquids*, 4th ed. ed., Elsevier, Amsterdam, 2013.
- (38) M. Neumann, Dipole moment fluctuation formulas in computer simulations of polar systems, *Mol. Phys.* 50 (1983) 841-845.
- (39) A. Truckymchuk, J. Alejandre, Computer simulations of liquid/vapor interface in Lennard-Jones fluids: some questions and answers, *J. Chem. Phys.* 111 (1999) 8510-8523.
- (40) P. Orea, J. López-Lemus, J. Alejandre, Oscillatory surface tension due to finite size effects, *J. Chem. Phys.* 123 (2005) 114702-114813.

- (41) M. Gonzalez-Melchor, F. Bresme, J. Alejandre, Molecular dynamics simulations of the surface tension of ionic liquids, *J. Chem. Phys.* 122 (2005) 104710-104718.
- (42) R. Garcia Fernández, J.L. Abascal, C. Vega, The melting point of ice Ih for common water models calculated from direct coexistence of the solid-liquid interface, *J. Chem. Phys.* 124 (2006) 144506.
- (43) V.F. Petrenko, R.W. Whitworth, *Physics of Ice*, Oxford University Press, Oxford, 1999.
- (44) K. Ichikawa, Y. Kameda, T. Yamaguchi, H. Wakita, M. Misawa, Neutron-diffraction investigation of the intramolecular structure of a water molecule in the liquid phase at high temperatures. *Mol. Phys.* 73 (1991) 79.
- (45) A. Zeidler, P.S. Salmon, H. E. Fischer, J. C. Neufeind, J. M. Simonson, T.E. Markland, Isotope effects in water as investigated by neutron diffraction and path integral molecular dynamics. *J. Phys.: Condens. Matter* 24 (2012) 284126.
- (46) A. H. Narten, H. A. Levy, *Liquid Water: Molecular Correlation Functions from X Ray Diffraction*. *J. Chem. Phys.* 55 (1971) 2263-2269.
- (47) B. Tomberli, C. J. Benmore, P. A. Egelstaff, J. Neufeind, V. Honkimaki, Isotopic quantum effects in water structure measured with high energy photon diffraction. *J. Phys.:Condens. Matter*. 12 (2000) 2597-2612.
- (48) E. W. Lemmon, M. O. McLinden, D. G. Friend, *Thermophysical Properties of Fluid Systems*, NIST Chemistry WebBook, NIST Standard Reference Database; Linstrom, P.J., Mallard, W.G., Eds.; 2005; <http://webbook.nist.gov> (accessed July 1, 2018).
- (49) J. López-Lemus, J. Alejandre, Thermodynamic and Transport Properties of Simple Fluids Using Lattice Sums: Bulk Phases and Liquid-Vapour Interface. *Mol. Phys.* 100 (2002) 2983-2992.

- (50) M. A. Gonzalez, J. L. F. Abascal, The Shear Viscosity of Rigid Water Models. *J. Chem. Phys.* 132 (2010) 096101-096102.
- (51) R. G. Fernández, J. L. F. Abascal, C. Vega, The Melting Point of Ice I for Common Water Models Calculated from Direct Coexistence of the Solid-Liquid Interface. *J. Chem. Phys.* 124 (2006) 144506-144518.